3D-2D Coupled Model for Eddy Currents in Laminated Iron Cores

Siegfried Vanaverbeke[1], Herbert De Gersem[1], Giovanni Samaey[2]
[1]Katholieke Universiteit Leuven, Wave Propagation and Signal Processing Research Group
Etienne Sabbelaan 53, 8500 Kortrijk, Belgium
sigfried.vanaverbeke@kuleuven-kortrijk.be; herbert.degersem@kuleuven-kortrijk.be
[2]Katholieke Universiteit Leuven, Department of Computer Science and Applied Mathematics
Celestijnenlaan 200A, 3000 Leuven, Belgium
giovanni.samaey@cs.kuleuven.be

***Abstract*— Eddy currents due to magnetic flux perpendicular to the sheets of a lamination iron core are represented on a number 2D slice models, which are embedded in a 3D model of the entire device. The choice of a different spatial resolution enables to attain a advantageous convergence of the discretisation error for the eddy-current power losses, compared to the standard modelling technique using an anisotropic surrogate material.**

I. Introduction

Eddy-current effects in laminated iron cores have a significant influence on the behaviour and performance of electrotechnical devices. We consider a local coordinate system (α, β, γ) where γ is perpendicular to the lamination sheets, whereas α and β are aligned with the plane in such way that the tangential component H_α of the magnetic field strength $\mathbf{H}$ and the tangential component J_β of the electric current density $\mathbf{J}$ are oriented along α and β. Two types of eddy-current paths are distinguished. The eddy currents $\mathbf{J} = (0, J_\beta, J_\gamma)$ closing at the lamination edges and caused by the major magnetic field components $\mathbf{H} = (H_\alpha, 0, 0)$ have been studied extensively, e.g. [1]–[4]. Here, we focus on the eddy currents due to the magnetic field component H_γ perpendicular to the laminates, typically occurring at the ends of the lamination stack. A widespread technique relies upon an anisotropic surrogate material derived from the parameters of the contributing materials and the fill factor of the stack [5], [6]. This technique has been successfully applied to machines [7] and transformers [8]. In [9], a coupling is set up between an overall 3D model and the 3D model of an individual lamination, which is capable of considering both types of eddy-current effects at the same time. This paper proposes an alternative to that and couples an overall 3D model with a number of 2D *slice* models which account for the complicated eddy-current paths in the lamination plane.

II. Multi-Scale Formulation and Discretisation

At a 3D model of the entire device (Fig. 1), a magnetoquasistatic (MQS) formulation in terms of the magnetic vector potential (MVP) is discretised by standard edge elements on tetrahedra or hexahedra (Fig. 2a). The eddy-current effects due to magnetic flux components aligned with the laminated plane are taken into account by the low-frequency approximation

$$\mathbf{H} = f(\mathbf{B}) + \frac{\sigma d^2}{12}\frac{\mathrm{d}\mathbf{B}}{\mathrm{d}t} \quad , \tag{1}$$

where $f()$ represent the BH-characteristic, $\mathbf{B}$ is the magnetic flux density, σ the conductivity and d the sheet thickness

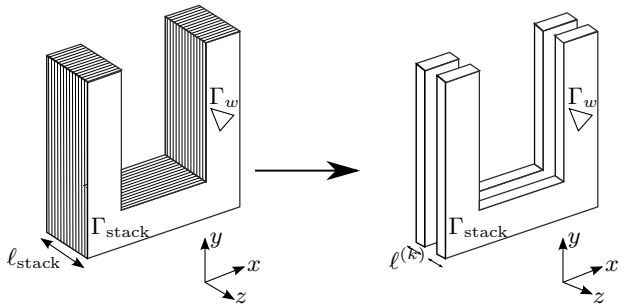

Fig. 1. Laminated core with cross-section Γ_{stack} and length ℓ_{stack}; homogenised slice with length $\ell^{(k)}$; control volume $\Gamma_m \otimes \ell^{(k)}$.

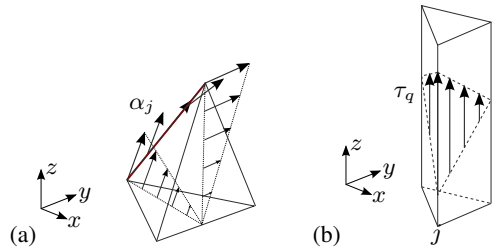

Fig. 2. (a) Lowest order edge function α_j on a tetrahedral grid and (b) lowest order longitudinal edge function τ_j on a trigonal prism.

[1]. A higher-order approximation [2], [10] could be built in as well. The lamination stack is subdivided in a number of slices covering a (non-necessarily integer) number of sheets (Fig. 1). A triangulation of the stack cross-section is extruded to establish a trigonally prismatic grid for each of the slices. At each slice, the MQS formulation in terms of the γ-component of the electric vector potential (EVP) is discretised by edge functions aligned with γ (Fig. 2b). The discrete coupled system of equations reads

$$\begin{bmatrix} \mathbf{A}_{\nu\xi\sigma} & -\mathbf{V}^{(k)} & 0 \\ 0 & \mathbf{A}^{(k)}_{\rho\mu} & s\mathbf{Q}^{(k)T}_{\mu} \\ -\mathbf{W}^{(k)} & \mathbf{Q}^{(k)}_{\mu} & \mathbf{\Lambda}^{(k)}_{\mu} \end{bmatrix} \begin{bmatrix} \widehat{\mathbf{a}} \\ \widehat{\mathbf{t}}^{(k)} \\ \widehat{\mathbf{h}}^{(k)}_{\mathrm{s}} \end{bmatrix} = \begin{bmatrix} \widehat{\widehat{\mathbf{j}}}_{\mathrm{s}} \\ 0 \\ 0 \end{bmatrix} \quad , \tag{2}$$

where $\mathbf{A}_{\nu\xi\sigma} = \mathbf{K}_\nu + s\mathbf{K}_\xi + s\mathbf{M}_\sigma$ and $\mathbf{A}^{(k)}_{\rho\mu} = \mathbf{K}^{(k)}_\rho + s\mathbf{M}^{(k)}_\mu$. The second and third system part is repeated for every slice k. $\mathbf{K}_\nu$ is the magnetic diffusion matrix, $\mathbf{K}_\xi$ is a diffusion matrix incorporating (1), $\mathbf{M}_\sigma$ the conductance matrix, $\widehat{\mathbf{a}}$ the degrees of freedom (DoFs) for the MVP and $\widehat{\widehat{\mathbf{j}}}_{\mathrm{s}}$ the discretisation for the applied currents. $\mathbf{K}_\rho$ is the electrokinetic diffusion matrix, $\mathbf{M}_\mu$ the permeance matrix and $\widehat{\mathbf{t}}^{(k)}$ the DoFs for the EVP in slice k. The submodels are coupled through the discrete source magnetic field $\widehat{\mathbf{h}}^{(k)}_{\mathrm{s}}$. The magnetic flux density $\mathbf{B} =$

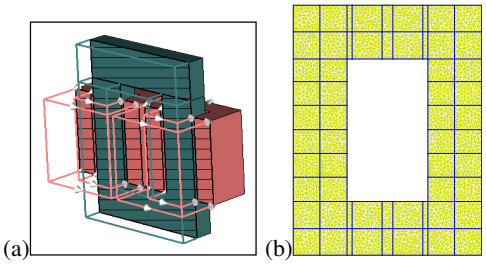

Fig. 3. 3D model and 2D slice models of a single-phase transformer. The rectangles indicate control volumes.

$\nabla \times \mathbf{A} = \mu \mathbf{H}_\mathrm{s} + \mu \mathbf{T}$ is forced to match between models in a weak way. For that purpose, a set of control volumes $\Omega_w^{(k)} = \Gamma_w \otimes [0, \ell^{(k)}]$ with Γ_w a patch in the lamination cross-section and $\ell^{(k)}$ the length of slice k, is defined. The third matrix equation in (2) is obtaining by weighting the equality for $\mathbf{B}$ by piecewise constant vectorial shape functions defined on $\Omega_w^{(k)}$ and oriented along the γ-direction.

The formulation is easily extended to the nonlinear case, i.e. $\mathbf{K}_\nu$, $\mathbf{Q}_\mu^{(k)}$, $\mathbf{M}_\mu^{(k)}$ and $\mathbf{\Lambda}_\mu^{(k)}$ need to be linearised. When the stack cross-section is not invariant along γ, it is a good idea to define a conformal transformation such that the approach of extruding a triangular grid can be maintained. The expected gain of this formulation is related to the fact that the 3D and 2D grids can be refined independently. The 3D grid is refined such that the variation of the magnetic flux density along γ is well resolved, whereas the 2D grid is chosen such that the skin depth along α- and β-directions is accommodated.

III. Application

The eddy-current losses at no-load operation of a single-phase transformer are calculated. As a reference, 3D model with a decreasing mesh size has been constructed, meshed and solved by the `CST EMStudio` software [11] (Fig. 3a). Thereby, an appropriate anisotropic surrogate model is implemented. The new approach makes use of the same 3D model and adds 2D slice models of the lamination stack of which the cross-section is meshed by `Triangle` [12] (Fig. 3b). A convergence test (Fig. 4) shows that the convergence order for the magnetic energy and the power losses is the same for both approaches. For the approach with embedded 2D slice models, the power losses converge with a larger convergence factor than for the standard technique. The convergence, however, does not get as good as the convergence for the magnetic energy. Eddy currents as they appear in two places in the lamination stack are plotted in Fig. 5.

IV. Conclusion

Eddy currents in the lamination plane can be accurately described on additional 2D models of slices of the lamination stack. Embedded in an overall 3D model, this dedicated modelling technique succeeds in substantially improving the convergence factor, as is shown for the example of a simple single-phase transformer.

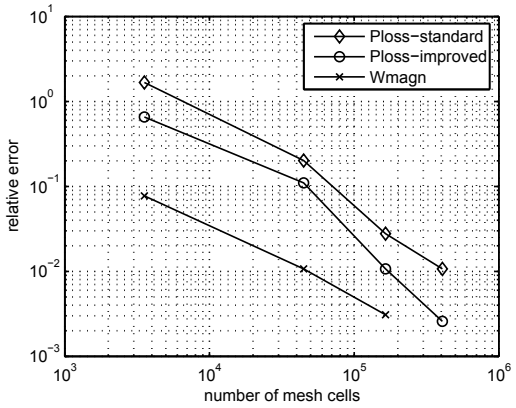

Fig. 4. Convergence of the relative error on the magnetic energy (`Wmagn`) and the eddy-current power loss (`Ploss`) w.r.t. the number of 3D grid cells. Comparison between a standard model with anisotropic surrogate material (`-standard`) and the improved model with 2D slice models (`-improved`).

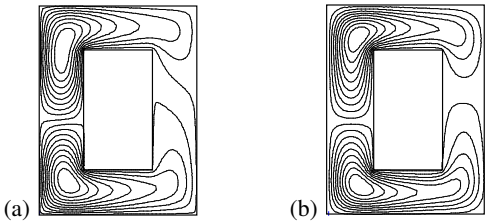

Fig. 5. Eddy-current distribution in the lamination stack: (a) at the front side and (b) 5.3 mm behind the front side of the lamination stack.

References

[1] J. Gyselinck, L. Vandevelde, J. Melkebeek, P. Dular, F. Henrotte, and W. Legros, "Calculation of eddy currents and associated losses in electrical steel laminations," *IEEE Trans. Magn.*, vol. 35, no. 3, pp. 1191–1194, May 1999.

[2] O. Bottauscio and M. Chiampi, "Analysis of laminated cores through a directly coupled 2-D/1-D electromagnetic field formulation," *IEEE Trans. Magn.*, vol. 38, no. 5, p. 23582360, Sept. 2002.

[3] L. Krähenbühl, P. Dular, T. Zeidan, and F. Buret, "Homogenization of lamination stacks in linear magnetodynamics," *IEEE Trans. Magn.*, vol. 40, no. 2, pp. 912–915, Mar. 2004.

[4] P. Dular, "A time-domain homogenization technique for lamination stacks in dual finite element formulations," *J. Comput. Appl. Math.*, vol. 215, pp. 390–399, 2008.

[5] H. Euler and T. Weiland, "Zur Berechnung der Wirbelströme in beliebig geformten, lamellierten, dreidimensionalen Eisenkörpern," *Archiv für Elektrotechnik*, vol. 61, pp. 103–109, 1979.

[6] V. Silva, G. Meunier, and A. Foggia, "A 3-D finite element computation of eddy currents and losses in laminated iron cores allowing for electric and magnetic anisotropy," *IEEE Trans. Magn.*, vol. 31, no. 3, p. 21392141, May 1995.

[7] J. Pippuri and A. Arkkio, "Time-harmonic induction-machine model including hysteresis and eddy currents in steel laminations," *IEEE Trans. Magn.*, vol. 45, no. 7, pp. 2981–2989, July 2009.

[8] E. Schmidt, P. Hamberger, and W. Seitlinger, "Calculation of eddy current losses in metal parts of power transformers," *COMPEL*, vol. 22, no. 4, pp. 1102–1114, 2003.

[9] K. Preis, O. Bíró, and I. Tiča, "FEM analysis of eddy current losses in nonlinear laminated iron cores," *IEEE Trans. Magn.*, vol. 41, no. 5, pp. 1412–1415, May 2005.

[10] J. Gyselinck, P. Dular, C. Geuzaine, and R. Sabariego, "Surface-impedance boundary conditions in time-domain finite-element calculations using the magnetic-vector-potential formulation," *IEEE Trans. Magn.*, vol. 45, no. 3, pp. 1280–1283, Mar. 2009.

[11] Computer Simulation Technology AG, "CST EM Studio," www.cst.com.

[12] J. Shewchuk, "Delaunay refinement algorithms for triangular mesh generation," *Computational Geometry*, vol. 22, no. 1-3, pp. 21–74, May 2002.